Title: Positioning errors of anatomical landmarks identified by fixed vertices in homologous meshes.

Words count:

Abstract (<=300):	297
Figures (12 + 46 + 13):	71
Tables (586 +588 + 348):	1522
References:	691
Manuscript length (<=3000):	2995
Total in docx file:	5576

Authors names and affiliations:

Ana V. Ruescas Nicolau[1] ✉ ana.ruescas@ibv.org

Helios De Rosario[1] ✉ helios.derosario@ibv.org

Eduardo Parrilla Bernabé[1] ✉ eduardo.parrilla@ibv.org

M.-Carmen Juan[2] ✉ mcarmen@dsic.upv.es

Corresponding author:

Ana V. Ruescas Nicolau

ana.ruescas@ibv.org

Permanent address:

[1] Instituto de Biomecánica - IBV. Universitat Politècnica de València, edifici 9C. Camí de Vera, s/n, 46022 València, Spain.

[2] Instituto Universitario de Automática e Informática Industrial. Universitat Politècnica de València, edifici 1F. Camí de Vera, s/n, 46022 València, Spain.

Title: Positioning errors of anatomical landmarks identified by fixed vertices in homologous meshes

Abstract

Background

Human movement analysis is usually achieved by tracking markers attached to anatomical landmarks with photogrammetry. Such marker-based systems have disadvantages that have led to the development of markerless procedures, although their accuracy is not usually comparable to that of manual palpation procedures. New motion acquisition systems, such as 3D temporal scanners, provide homologous meshes that can be exploited for this purpose.

Research question

Can fixed vertices of a homologous mesh be used to identify anatomical landmarks with an accuracy equivalent to that of manual palpation?

Methods

We used 3,165 human shape scans from the CAESAR dataset, with labelled locations of anatomical landmarks. First, we fitted a template mesh to the scans, and assigned a vertex of that mesh to 53 anatomical landmarks in all subjects. Then we defined a nominal vertex for each landmark, as the more centred vertex out of the set assigned for that landmark. We calculated the errors of the template-fitting and the nominal vertex determination procedures, and analysed their relationship to subject's sex, height and body mass index, as well as their size compared to manual palpation errors.

Results

The template-fitting errors were below 5 mm, and the nominal vertex determination errors reached maximum values of 26 mm. Except for the trochanter, those errors were the same order of magnitude or smaller than inter-examiner errors of lower limb landmarks. Errors increased with height and body mass index, and were smaller for men than for women of the same height and body mass index.

Significance

We defined a set of vertices for 53 anatomical landmarks in a homologous mesh, which yields location errors comparable to those obtained by manual palpation for the majority of landmarks. We also quantified how the subject's sex and anthropometric features can affect the size of those errors.

Keywords

1. Introduction

The identification of anatomical landmarks (AL) in human movement analysis is a widely studied issue, since it affects the position and orientation accuracy in the anatomical frames definition, and the subsequent analysis of joints kinematics [1].

In marker-based systems, AL are usually identified by a manual palpation procedure performed by an expert examiner. Those methods often involve attaching markers that can restrict

movements and their spontaneity, are time-consuming and may require a tedious calibration task [2].

New developments for human motion capture systems are focused on markerless systems, which avoid those issues [3–7]. One of them is Move4D/IBV (Instituto de Biomecánica IBV, Spain), which provides homologous meshes combining artificial intelligence methods and a template-fitting procedure. The homologous mesh is a watertight, closed-surface, with point-to-point correspondence between subjects and along the movement sequence [8]. That system has been successfully used in gait analysis, identifying AL as specific mesh vertices [9]. However, for a practical application, the correspondence between the AL and the mesh vertices should be an automatic process.

In the field of anthropometry, 3D body scanners have allowed the acquisition of large databases. The Civilian American and European Surface Anthropometry Resource dataset (CAESAR) contains 3D scans, AL location files and manual measurements of more than 4,000 people in different poses [10]. The raw scans of the CAESAR database can be mapped to the homologous mesh through template-fitting methods [11], in order to use the information of the labelled AL as a source of data to select the optimal vertex to represent each landmark.

The aim of this study is to determine the accuracy of identifying AL automatically as fixed vertices of a homologous mesh. To achieve that, we computed and analysed the distances between the labelled AL locations in the CAESAR database and the homologous mesh vertices that better represent the same ALs for that population.

2. Methods

2.1. Subjects

This study used data from the CAESAR database. We selected a group composed of 3D scans of 3,165 subjects from USA and Italy performing the "A-pose" (upright with legs and arms slightly apart). This group of subjects is the biggest homogeneous group in CAESAR database, measured with the same scanning and landmarking systems [10].

The selected group was composed of 1,530 male and 1,635 female subjects, with age 37.31 ± 12.66 years, weight 74.08 ± 18.94. kg, height 1,700.09 ± 103.21 mm, and body mass index (BMI) 25.46 ± 5.42 kg/m^2.

2.2. Calculation of the homologous mesh

Some data processing was needed previous to transforming the raw data from the 3D scans into the homologous mesh (e.g. erasing the fingers A-pose of the CAESAR scans because the homologous mesh had closed cuffs as shown in Figure 1). This transformation is an automatic process in which an algorithm adjusts the homologous mesh to a point cloud [12] using two templates with symmetric topologies for men and women. The symmetry ensured that each vertex in the mesh had its symmetric counterpart, except for those that lie in the sagittal plane. That mesh had an average length of the polygon edge around 5 mm (ALPE$_5$).
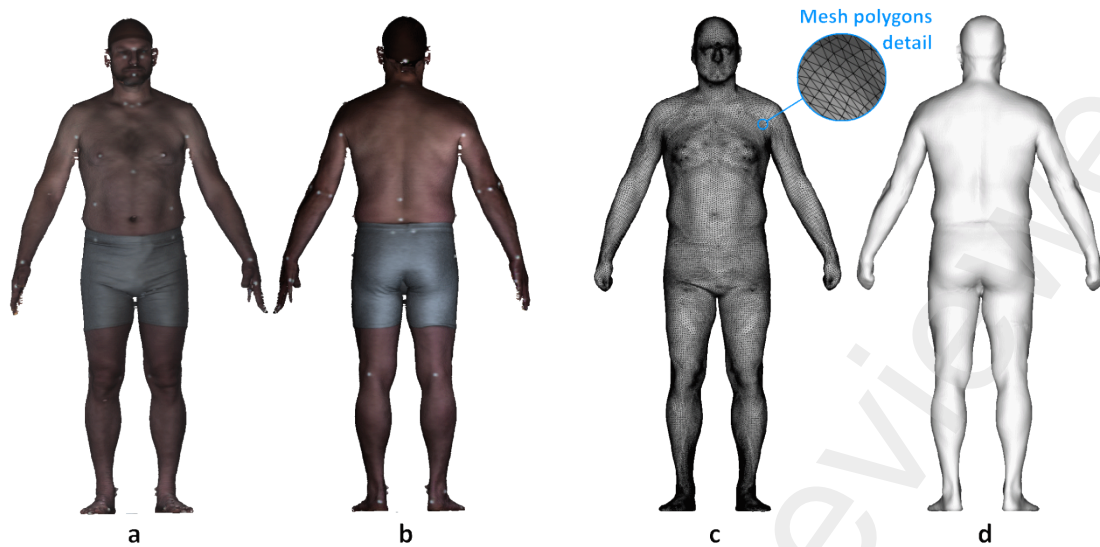
Figure 1. Raw scan mesh file (a-b) and corresponding homologous mesh (c-d).

2.3. Identification of AL on the homologous mesh

We studied the 53 ALs shown in Figure 2, out of the 73 landmarks available in the CAESAR database, considering their interest in biomechanics, since they are often used in kinematic analysis or for the body parts segmentation[13]. Three vertices were assigned to each AL on the homologous mesh, as defined in the following subsections.

2.3.1. Closest vertices determination

The closest vertices (CV) were the subject-specific mesh vertices corresponding to the 53 AL, defined as the best possible representation of the AL that might be located on the fitted homologous mesh. Each CV was determined as the vertex whose coordinates minimized the distance to the corresponding labelled point in the CAESAR dataset. For landmarks whose location was near the sagittal plane (e.g. on the spine, middle of the head or the torso), the CV was forced to lie on the body's line of symmetry of the mesh.

2.3.2. Nominal vertices determination

Two nominal vertices were calculated for each AL, defined as the best common representations of the AL on the homologous mesh: the asymmetric nominal vertices (ANV), which did not consider any relationship between different AL, and the symmetric nominal vertices (SNV), which enforced a symmetric relationship between AL that had a contralateral (left-right) counterpart (bilateral AL). Those vertices were calculated independently for men and women.

In order to calculate the nominal vertices, the distance between any two vertices of the mesh was defined as the length of the shortest path that connected those vertices following the mesh edges, calculated by the "Shortest Path Faster Algorithm" as implemented in [14]. For a given set of vertices of the mesh, its central point was defined as the vertex with the minimum sum of squared distances to all the other vertices. The SNV and ANV were calculated as the centers of different sets of vertices:

- For the ANV of all AL, and for the SNV of AL lying on the body's plane of symmetry, the sets of vertices were the collections of their corresponding CV.
- For the SNV of bilateral AL, those sets were expanded with the symmetric vertices of the CV associated to the contralateral landmarks.
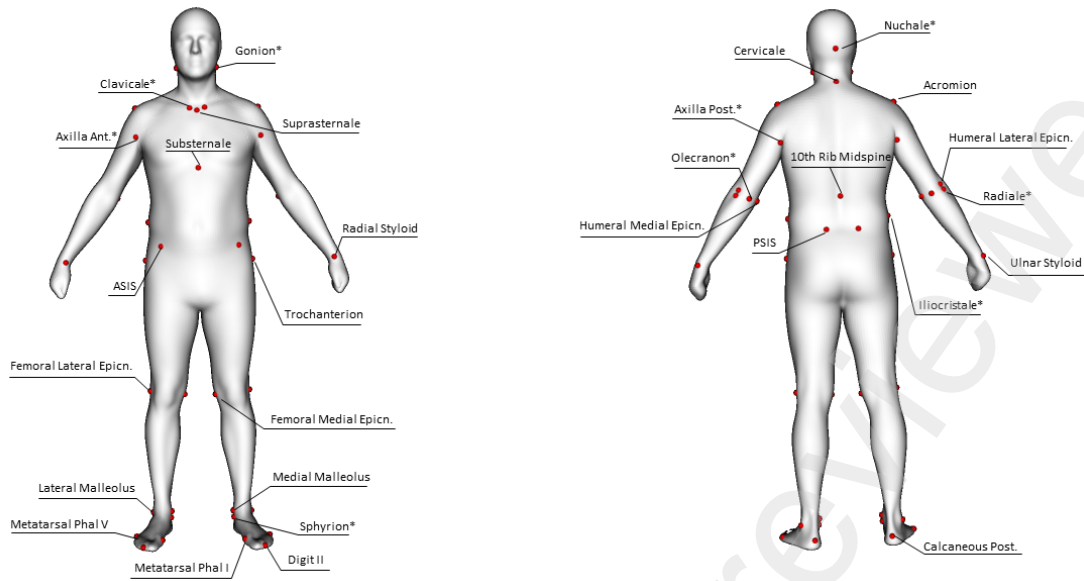
Figure 2. Selected AL. All landmarks except Suprasternale, Substernale, Nuchale, Cervicale and 10th Rib Midspine had left and right counterparts. AL marked with an asterisk are used for the segmentation of body parts according to [13], but are not usually employed for analysis of human movements.

2.4. Statistical analysis

In a few samples of the CAESAR dataset, some AL were mislabelled. We discarded those data points using the next procedure to detect them.

The set of distances between the CV and the SNV were sorted in ascending order, $\{d_0, d_1,...,d_n\}$ for each AL, such that $d_i \leq d_{i+1}$. Then, a cluster of "small distances" was defined as the lower range of distances $\{d_0, d_1,...,d_s\}$ without "gaps" that exceed half the size of the previous distance. In formal terms, that cluster included d_0 and the values d_i such that if $i \leq s$, any of the following must be true:

a. $d_{i-1} = 0$, or
b. $d_i < 1.5 d_{i-1}$.

All the vertices whose distance was greater than d_s were ruled out from the subsequent analyses as outliers.

2.4.1. Description of errors

There were two sources of discrepancy between the positions of the labelled AL and the ones identified by their SNV on the homologous mesh:

- The distortion of raw data produced by the template-fitting procedure, which was expected to be of the order of magnitude of the $ALPE_5$. This was quantified as the distance between the CV of the AL and its labelled position in the dataset (CV-LBL).
- Uncertainty in the optimal vertex determination, due to morphological differences between subjects. This was quantified by the distance between the SNV and the CV (SNV-CV).

We described those error components distributions by their mean and standard deviations. Those errors were calculated separately for the medial-lateral (ML), vertical (V) and anterior-posterior (AP) axes.

The right and left distributions of bilateral AL were pooled up for the analysis, assuming that they were symmetric. In order to verify that assumption, we calculated the differences between right- and left-side errors (their sum in the ML direction), and compared the mean of those differences with their pooled standard deviation. This was also done for distances between ANV and CV. Our hypothesis was that the mean differences would be of the order of magnitude of the ALPE$_5$, and smaller than the pooled standard deviations, and that the results would be the same for ANV-CV and SNV-CV errors.

2.4.2. Statistical modelling

We considered that error distributions might depend on the characteristics of the subjects. That relationship was quantified with a Generalized Linear Model with Varying Dispersion [15], using the "dglm" package for R [16], which fits two sub-models: the "mean model" that adjusted the expected value of the error, and the "dispersion model" that adjusted its variance. The model related the error in the X, Y, Z coordinates to the height and BMI of the subjects, considering that the dispersion of the error could also depend on the same characteristics, as well as on the sex. The expected values of the errors were assumed to follow a Gaussian distribution, and the log function was used as link between the dispersion parameter and its linear predictor.

The sizes of those effects were assessed by the value $\exp\left(\frac{\gamma_v}{2}\sigma_v\right)$, where γ_v are the coefficients of the dispersion model, and σ_v are the standard deviations of the corresponding variables, which was set to the unity for sex. (See the supplementary material for the reasoning of those calculations).

3. Results

Table 1 shows the results of the error differences for bilateral AL in the symmetry analysis.

The mean differences of CV-LBL errors were usually smaller than 1 mm, and always smaller than 2 mm, with a maximum of 1.4 mm in the ML axis for Trochanterion.

The mean differences of ANV-CV errors were smaller than the ALPE$_5$.

The mean differences of SNV-CV errors were smaller than the ALPE$_5$ for the vast majority of markers in the ML and V axes, but greater in the AP axis for 6 out of the 24 bilateral landmarks, the greatest difference being for the Trochanterion (10.5 mm).

The mean differences of the errors were usually one order of magnitude smaller than their pooled standard deviations (SD), except for the SNV-CV error of some AL in the directions for which they exceeded the ALPE$_5$ (ASIS in the ML axis; Humeral Lateral Epic. and Radiale in the V axis; and Acromion, ASIS, Femoral Lateral Epicn., Gonion, Iliocristale and Trochanterion in the AP axis).

Table 1. Mean of left/right-side differences, and pooled standard deviation of the errors for bilateral AL. All values in mm.

Marker	Error type	Diff. ML error Mean (SD)	Diff. V error Mean (SD)	Diff. AP error Mean (SD)
Acromion	CV-LBL	0.5 (3.7)	0.2 (3.3)	0.0 (2.8)
	ANV-CV	2.4 (11.0)	-1.9 (10.8)	-0.2 (9.1)
	SNV-CV	3.0 (11.2)	-3.1 (10.9)	-7.8 (9.1)
ASIS	CV-LBL	0.6 (1.6)	0.0 (1.5)	0.8 (1.6)
	ANV-CV	2.5 (10.3)	-0.8 (17.9)	-1.7 (11.0)
	SNV-CV	7.5 (10.6)	1.8 (17.9)	-5.7 (11.3)
Axilla Ant.	CV-LBL	0.4 (2.0)	-0.1 (1.9)	0.3 (1.3)
	ANV-CV	-1.0 (8.8)	3.4 (16.7)	0.3 (5.0)

	SNV-CV	3.6 (8.7)	0.9 (17.4)	-0.1 (4.5)
Axilla Post.	CV-LBL	-0.2 (2.1)	0.0 (2.2)	-0.1 (1.3)
	ANV-CV	1.3 (7.9)	3.4 (12.8)	-1.0 (3.7)
	SNV-CV	-1.0 (7.8)	-0.1 (12.9)	-0.2 (3.6)
Calcaneous Post.	CV-LBL	-0.2 (1.4)	0.1 (1.3)	-0.7 (1.4)
	ANV-CV	-0.5 (4.8)	0.2 (7.0)	0.2 (1.6)
	SNV-CV	-0.5 (4.8)	0.2 (7.0)	0.2 (1.6)
Clavicale	CV-LBL	0.1 (2.2)	0.1 (1.6)	0.3 (1.3)
	ANV-CV	-1.5 (5.8)	-4.8 (6.8)	3.5 (4.3)
	SNV-CV	0.3 (6.0)	1.2 (6.9)	-0.5 (4.4)
Digit II	CV-LBL	-0.5 (2.4)	0.2 (1.8)	-0.3 (2.6)
	ANV-CV	0.2 (5.3)	0.6 (3.5)	-0.1 (4.4)
	SNV-CV	0.1 (5.3)	2.5 (3.4)	-0.6 (4.4)
Femoral Lateral Epicn.	CV-LBL	-1.3 (1.3)	0.2 (1.7)	-0.5 (1.6)
	ANV-CV	0.4 (2.2)	0.4 (10.5)	-1.5 (8.0)
	SNV-CV	1.1 (2.2)	-3.1 (10.2)	-7.2 (7.9)
Femoral Medial Epicn.	CV-LBL	0.1 (1.1)	0.0 (1.8)	0.0 (1.6)
	ANV-CV	-0.2 (3.6)	-0.6 (10.4)	-0.2 (9.1)
	SNV-CV	0.5 (3.6)	-0.6 (10.4)	2.7 (9.3)
Gonion	CV-LBL	0.3 (1.7)	-0.1 (1.5)	-0.3 (1.5)
	ANV-CV	-0.1 (3.4)	0.1 (6.9)	-0.8 (7.7)
	SNV-CV	-0.5 (3.3)	-0.8 (6.9)	-5.7 (7.6)
Humeral Lateral Epicn.	CV-LBL	0.2 (1.7)	0.0 (2.7)	-0.1 (1.5)
	ANV-CV	-0.5 (7.5)	0.0 (9.3)	-0.4 (6.1)
	SNV-CV	-2.6 (7.5)	-5.6 (9.0)	-3.2 (6.3)
Humeral Medial Epicn.	CV-LBL	-1.1 (2.0)	-0.7 (2.5)	-1.0 (1.9)
	ANV-CV	-1.7 (6.8)	1.1 (8.5)	-0.5 (9.3)
	SNV-CV	-1.7 (6.8)	1.1 (8.5)	-0.5 (9.3)
Iliocristale	CV-LBL	1.0 (3.1)	0.3 (2.0)	0.3 (1.8)
	ANV-CV	-0.5 (5.6)	-1.0 (18.1)	-0.6 (13.8)
	SNV-CV	0.1 (5.7)	-1.0 (17.9)	-6.4 (14.0)
Lateral Malleolus	CV-LBL	0.9 (1.5)	0.0 (1.1)	-0.4 (1.4)
	ANV-CV	0.6 (2.6)	-0.3 (5.2)	0.7 (5.0)
	SNV-CV	-0.5 (2.5)	-2.3 (5.3)	-1.5 (5.1)
Medial Malleolus	CV-LBL	1.3 (3.4)	0.2 (1.5)	-0.1 (1.4)
	ANV-CV	0.3 (1.3)	-1.3 (6.3)	-0.7 (6.4)
	SNV-CV	0.2 (1.3)	0.5 (6.4)	-2.4 (6.5)
Metatarsal Phal. I	CV-LBL	0.9 (2.8)	-0.3 (1.5)	-0.5 (2.2)
	ANV-CV	-0.5 (2.1)	1.1 (4.3)	-2.8 (6.7)
	SNV-CV	-0.5 (2.1)	1.1 (4.3)	-2.8 (6.7)
Metatarsal Phal. V	CV-LBL	0.2 (1.9)	0.0 (1.7)	-0.2 (1.7)
	ANV-CV	-0.7 (3.2)	1.1 (3.4)	-0.4 (8.1)
	SNV-CV	1.2 (3.1)	-1.1 (3.0)	1.8 (8.0)
Olecranon	CV-LBL	-0.1 (2.1)	-0.2 (1.9)	-0.4 (1.3)
	ANV-CV	0.1 (8.5)	0.9 (8.6)	-0.6 (3.1)
	SNV-CV	-3.1 (8.6)	-4.3 (8.5)	0.9 (3.1)

Marker	Error type			
PSIS	CV-LBL	0.0 (1.8)	-0.4 (1.6)	0.7 (1.1)
	ANV-CV	2.8 (13.1)	-0.1 (15.7)	0.2 (7.8)
	SNV-CV	-3.2 (13.4)	-0.8 (15.7)	-0.7 (7.9)
Radial Styloid	CV-LBL	0.2 (1.5)	-0.2 (2.3)	-0.6 (1.6)
	ANV-CV	1.5 (5.8)	0.2 (7.8)	0.4 (3.4)
	SNV-CV	3.4 (6.0)	0.4 (7.8)	0.5 (3.4)
Radiale	CV-LBL	0.2 (1.7)	0.1 (2.4)	-0.1 (1.4)
	ANV-CV	-0.9 (7.7)	-0.9 (8.7)	-1.3 (5.8)
	SNV-CV	-2.6 (7.5)	-6.1 (8.5)	-4.3 (6.1)
Sphyrion	CV-LBL	1.2 (3.0)	0.0 (1.4)	-0.1 (1.3)
	ANV-CV	0.2 (1.4)	-0.6 (7.2)	1.0 (7.1)
	SNV-CV	-0.3 (1.5)	0.8 (7.2)	-3.5 (7.3)
Trochanterion	CV-LBL	1.4 (2.4)	0.2 (1.5)	0.3 (2.2)
	ANV-CV	0.4 (3.2)	-0.7 (21.1)	0.1 (13.9)
	SNV-CV	1.4 (3.3)	-1.9 (21.2)	-10.5 (14.2)
Ulnar Styloid	CV-LBL	-0.1 (1.5)	0.0 (1.4)	0.2 (1.1)
	ANV-CV	-0.1 (6.4)	0.6 (7.7)	0.3 (2.8)
	SNV-CV	1.2 (6.4)	-3.0 (8.3)	1.1 (2.8)

The mean CV-LBL errors and most of their SD (Table 2) were under the ALPE$_5$. Some SD in the ML axis (Acromion, Medial Malleolus, Metatarsal Phal. I, Sphyrion, Substernale, Nuchale and Cervicale) had a value slightly greater than the ALPE$_5$, with a maximum 3D value of 7.7 mm.

The SNV-CV errors were greater in comparison to CV-LBL: in the ML axis the SD errors were between [0.6, 13.4] mm in the ML axis, between [3.0, 21.2] mm in the V axis, and between [1.6, 15.1] mm in the AP axis. The SD of the 3D errors were in the range [7.8, 26.2] mm. In the worst cases, that was from 3 to 5 times the ALPE$_5$.

Table 2. Description of the errors in ML, V and AP axes for the coordinates of the closest vertices versus labelled positions (CV-LBL), and for nominal versus closest vertices (SNV-CV). All values in mm. (*): AL with a volumetric marker attached on the original raw scan files. (**): AL that lie on the sagittal plane.

Marker	Error type	ML error Mean (SD)	V error Mean (SD)	AP error Mean (SD)	3D SD error
Acromion*	CV-LBL	0.3 (5.4)	-4.6 (3.3)	0.4 (2.8)	6.9
	SNV-CV	1.5 (11.3)	-1.1 (11.0)	1.4 (9.9)	18.6
ASIS	CV-LBL	0.3 (1.6)	0.0 (1.5)	-0.1 (1.6)	2.8
	SNV-CV	3.7 (10.9)	3.1 (18.1)	3.1 (11.6)	24.1
Axilla Ant.	CV-LBL	0.2 (2.0)	0.1 (1.9)	-0.6 (1.3)	3.0
	SNV-CV	1.8 (8.8)	3.1 (17.3)	-1.0 (4.5)	20.0
Axilla Post.	CV-LBL	-0.1 (2.1)	0.1 (2.2)	0.3 (1.3)	3.3
	SNV-CV	-0.5 (7.9)	2.8 (12.9)	-1.3 (4.4)	15.8
Calcaneous Post.	CV-LBL	-0.1 (1.4)	-0.1 (1.3)	0.6 (1.4)	2.4
	SNV-CV	-0.2 (4.9)	-0.9 (7.0)	-0.6 (1.6)	8.7
Clavicale	CV-LBL	0.1 (2.3)	-0.1 (1.6)	-0.3 (1.3)	3.1
	SNV-CV	0.1 (6.0)	-3.3 (7.1)	1.9 (4.5)	10.3
Digit II	CV-LBL	-0.2 (2.9)	-0.2 (1.8)	-2.2 (2.6)	4.3
	SNV-CV	0.0 (5.3)	-1.1 (3.6)	-0.2 (4.4)	7.8
Femoral Lateral Epicn.	CV-LBL	-0.6 (1.4)	0.0 (1.7)	-0.1 (1.6)	2.7

	SNV-CV	0.5 (2.2)	-2.8 (10.3)	-0.9 (8.7)	13.7
Femoral Medial Epicn.	CV-LBL	0.1 (1.2)	0.1 (1.8)	-0.1 (1.6)	2.7
	SNV-CV	0.2 (3.9)	0.0 (10.4)	-0.5 (9.4)	14.6
Gonion	CV-LBL	0.1 (1.7)	0.1 (1.5)	0.0 (1.5)	2.7
	SNV-CV	-0.3 (3.3)	0.5 (6.9)	0.1 (8.2)	11.2
Humeral Lateral Epicn.	CV-LBL	0.1 (1.7)	-0.1 (2.7)	0.4 (1.5)	3.5
	SNV-CV	-1.3 (7.5)	-0.4 (9.4)	-0.5 (6.5)	13.7
Humeral Medial Epicn.	CV-LBL	-0.5 (2.1)	0.3 (2.5)	0.5 (2.0)	3.8
	SNV-CV	-0.8 (6.9)	-0.3 (8.5)	-1.3 (9.4)	14.4
Iliocristale*	CV-LBL	0.5 (4.7)	-0.8 (2.0)	0.0 (1.8)	5.5
	SNV-CV	0.1 (6.2)	-3.7 (17.9)	-3.7 (14.4)	23.8
Lateral Malleolus	CV-LBL	0.5 (1.7)	0.0 (1.1)	0.5 (1.4)	2.5
	SNV-CV	-0.2 (2.7)	0.0 (5.4)	0.7 (5.1)	7.9
Medial Malleolus*	CV-LBL	0.6 (7.5)	-0.5 (1.5)	-0.4 (1.4)	7.7
	SNV-CV	0.1 (2.9)	-1.2 (6.4)	1.1 (6.6)	9.7
Metatarsal Phal. I*	CV-LBL	0.4 (5.8)	-1.7 (1.5)	-1.7 (2.2)	6.4
	SNV-CV	-0.3 (2.1)	0.1 (4.3)	0.8 (6.8)	8.3
Metatarsal Phal. V	CV-LBL	0.1 (2.1)	-0.5 (1.7)	0.3 (1.7)	3.2
	SNV-CV	0.6 (3.3)	0.6 (3.0)	-1.6 (8.0)	9.2
Olecranon	CV-LBL	-0.1 (2.1)	0.1 (1.9)	0.5 (1.4)	3.1
	SNV-CV	-1.5 (8.7)	-1.7 (8.8)	-0.4 (3.7)	12.9
PSIS	CV-LBL	0.0 (1.8)	0.0 (1.6)	0.0 (1.2)	2.6
	SNV-CV	-1.6 (13.4)	1.3 (15.8)	0.1 (8.4)	22.3
Radial Styloid	CV-LBL	0.1 (1.5)	0.0 (2.3)	-0.2 (1.6)	3.1
	SNV-CV	1.7 (6.0)	-3.0 (7.8)	1.8 (3.4)	10.4
Radiale	CV-LBL	0.1 (1.7)	0.1 (2.4)	-0.3 (1.4)	3.3
	SNV-CV	-1.3 (7.5)	-0.4 (9.0)	-2.0 (6.5)	13.4
Sphyrion*	CV-LBL	0.6 (6.4)	0.6 (1.4)	-0.4 (1.3)	6.7
	SNV-CV	-0.2 (1.7)	-0.8 (7.2)	0.3 (7.5)	10.5
Trochanterion*	CV-LBL	0.7 (4.3)	-0.4 (1.5)	0.0 (2.2)	5.1
	SNV-CV	0.7 (3.4)	-0.4 (21.2)	4.2 (15.1)	26.2
Ulnar Styloid	CV-LBL	0.0 (1.5)	0.0 (1.4)	0.5 (1.1)	2.3
	SNV-CV	0.6 (6.4)	-0.3 (8.4)	-0.3 (2.9)	11.0
Suprasternale**	CV-LBL	0.5 (4.3)	-0.1 (1.5)	0.0 (1.1)	4.7
	SNV-CV	-0.1 (0.9)	-1.9 (7.9)	1.1 (5.1)	9.4
Substernale**	CV-LBL	4.7 (5.6)	0.0 (2.1)	-0.2 (1.2)	6.1
	SNV-CV	0.1 (0.9)	0.6 (17.2)	0.2 (6.4)	18.3
Nuchale**	CV-LBL	-4.8 (6.0)	0.0 (2.6)	0.5 (1.8)	6.8
	SNV-CV	-0.1 (0.9)	0.8 (12.4)	-1.5 (6.8)	14.1
Cervicale**	CV-LBL	-3.4 (5.3)	0.0 (1.9)	0.1 (1.5)	5.9
	SNV-CV	-0.1 (0.6)	1.7 (7.5)	1.0 (5.2)	9.2
10th Rib Midspine**	CV-LBL	-4.1 (4.9)	-0.1 (2.8)	-0.1 (1.4)	5.8
	SNV-CV	0.0 (1.1)	0.3 (19.8)	1.0 (5.2)	20.5

Table 3 shows the coefficients of the dispersion model that parametrizes the relationship between subject characteristics and SNV-CV errors. The coefficients for height and BMI were always greater than the unity, and their mean value was around 1.05 for height and 1.1 for BMI

in all directions. On the other hand, the coefficients for sex were usually smaller than 1, with mean value around 0.89 in the ML axis and 0.96 in the V and AP axes.

Table 3. Coefficients of the dispersion model that parametrizes the relationship between subject characteristics and SNV-CV errors in the ML, V and AP axes.

Landmark	ML			V			AP		
	Sex	Height	BMI	Sex	Height	BMI	Sex	Height	BMI
Acromion	0.985	1.049	1.230	0.819	1.106	1.164	1.138	1.023	1.088
ASIS	0.907	1.037	1.141	0.842	1.028	1.059	0.936	1.018	1.398
Axilla Ant.	0.820	1.049	1.103	1.020	1.072	1.210	1.142	1.096	1.187
Axilla Post.	0.810	1.062	1.107	0.848	1.078	1.118	0.697	1.187	1.113
Calcaneous Post.	1.142	1.014	1.102	0.942	1.115	1.002	1.031	1.009	1.022
Clavicale	0.964	1.051	1.036	1.035	1.017	1.067	0.844	1.031	1.033
Digit II	1.080	1.021	1.068	1.170	1.007	1.049	0.931	1.033	1.076
Femoral Lateral Epicn.	0.982	1.045	1.041	0.772	1.061	1.071	0.787	1.028	1.065
Femoral Medial Epicn.	0.843	1.040	1.243	0.757	1.064	1.052	0.728	1.073	1.223
Gonion	0.996	1.025	1.078	1.023	1.070	1.120	1.089	1.005	1.060
Humeral Lateral Epicn.	0.814	1.005	1.049	0.960	1.066	1.062	1.145	0.999	1.107
Humeral Medial Epicn.	0.730	1.057	1.214	0.970	1.037	1.088	0.813	1.037	1.088
Iliocristale	0.358	1.183	1.153	0.848	1.072	1.110	1.303	1.008	1.158
Lateral Malleolus	0.939	1.035	1.072	0.940	1.081	1.069	0.953	1.024	1.027
Medial Malleolus	0.916	1.013	1.029	0.948	1.050	1.040	0.815	1.031	1.111
Metatarsal Phal. I	0.918	1.044	1.079	1.002	1.044	0.999	0.931	1.050	1.055
Metatarsal Phal. V	1.017	1.040	0.972	0.997	1.022	1.049	1.020	1.018	1.054
Olecranon	0.877	1.039	1.131	1.093	1.044	1.033	0.548	1.097	1.143
PSIS	1.035	1.092	1.257	1.042	1.111	1.162	1.052	1.100	1.179
Radial_Styloid	0.907	1.034	1.133	0.862	1.065	1.090	1.242	1.031	1.116
Radiale	0.783	1.007	1.094	0.969	1.081	1.037	1.338	1.003	1.113
Sphyrion	0.979	1.023	0.992	0.974	1.054	1.020	0.812	1.040	1.084
Trochanterion	0.718	1.094	1.088	0.713	1.074	1.095	0.853	1.058	1.160
Ulnar Styloid	0.827	1.027	1.128	1.005	1.037	1.066	1.038	1.049	1.272
Suprasternale	0.860	1.037	1.077	1.116	1.027	1.098	0.913	1.053	1.044
Substernale	0.893	1.037	1.233	1.138	1.028	1.032	1.102	1.016	1.325
Nuchale	0.954	1.000	1.174	1.046	1.077	1.171	0.687	1.022	1.114
Cervicale	0.947	1.026	1.022	0.930	1.031	0.973	0.870	1.083	1.112
10th Rib Midspine	0.935	1.039	1.218	0.975	1.020	1.185	0.968	0.973	1.416

4. Discussion

The dispersion of the SNV positions on the homologous mesh and their distances to the AL labelled positions were due to the accumulation of errors coming from the source data and those derived from our procedure. According to [17], the labelling process of the source data consisted in picking manually the centre of the landmark identified by a 12 mm diameter sticker and then converting its position into 3-dimensional coordinates. This involved errors due to the manual positioning of the stickers and their digitization, whose magnitude could not be assessed.

4.1. Symmetry errors analysis

The symmetry analysis showed that right/left-hand side differences in CV-LBL errors were, in general, very small. We found that the differences in ANV-CV errors were small too, which meant that the ANV were centred in the distributions of their corresponding CV.

The mean differences in SNV-CV errors, on the other hand, were greater than the $ALPE_5$ in some AL. This meant that the distributions of those bilateral AL in the raw scans were not symmetric, so enforcing the symmetry in the definition of the symmetric nominal vertices led to increased error sizes.

It should be considered that the symmetric templates that we used were designed to model persons without amputations or pathologies that might affect the shape of their body unilaterally.

4.2. Template-fitting processing errors

The template-fitting errors (CV-LBL), were calculated as the distances from labelled points location in the CAESAR dataset to the CV. The mean errors were generally between ±1 mm, except for the Acromion in the V axis, Metatarsal Phal. I in the V and AP axes, Digit II in the AP axis, and four markers lying on the symmetry plane (Substernale, Nuchale, Cervicale and 10th Rib Midspine) in the ML axis.

For the first three AL that could be an artefact of the original labelling in the CAESAR dataset: the first two AL were identified by volumetric markers, and that might have influenced the accuracy in the labelling, as the human shape surface was occluded in the raw scans. On the other hand, the labelling process of the Digit II landmark (the toe tip) could have been affected because that area usually lacks data in the raw scans (Figure 3).

Figure 3. Foot scan quality in raw scan files in the CAESAR dataset.

In the case of the AL on the symmetry plane, the greater CV-LBL mean error could be due to the enforcement of CV to lie on the medial line of the homologous mesh, since that symmetry might not happen in the raw data (e.g. misaligned head or torso orientations).

The CV-LBL errors dispersion (SD) was generally smaller than the $ALPE_5$. That result was consistent with our definition of the CV, which was expected to lie at a maximum distance of one mesh polygon from the labelled points. The errors that were the same magnitude of the $ALPE_5$ or greater, corresponded to those that were attached with volumetric markers and, those that lied on the symmetry plane.

4.3. SNV determination errors

The uncertainty of SNV positions (SNV-CV distances) was greater than the template-fitting errors. The mean SNV-CV distances in all axes were still smaller than the $ALPE_5$, but their dispersion (SD) was three times the $ALPE_5$ or greater for more than half of the AL. This meant that the CV could be expected to be around the SNV, typically 3 vertices away from it.

We found no single set of reference values to compare the size of those errors for all landmarks. Reliability studies of AL positioning by palpation differ in the set of AL that were considered, as well as in the magnitude of the resulting errors, with [18] (focused on lower limb) and [19] (full

body) reporting generally greater errors than [20] (focused on upper limb) and [21] (full body). That variation could be due to the differences in the design of the experiments (number of subjects and examiners, subjects group characteristics, kind of measuring technology, etc.) and of the protocols used to measure inter-examiner errors.

The 3D size of SNV-CV distances in our study was the same order of magnitude as the 3D inter-examiner error in [18] and [19], except for the Trochanterion (26.2 mm in our study versus 17.7 mm in [18]). On the other hand, the dispersion of our errors was from 2 to 3 times greater than the errors reported in [20] and [21].

Another study assessed the error of estimating AL locations with a supervised learning method, using the same source of data from the CAESAR database as in our study [22]. The 3D dispersion of the SNV-CV errors in our study were about two times the size reported in [22] for Acromion, and 30% bigger for Axilla Ant. and Trochanterion. On the other hand, PSIS errors in our study was significantly smaller (22.3 mm versus 55 mm in [22]). The rest of AL location errors were the same magnitude or slightly bigger as ours.

4.4. Dependencies of error size on sex and anthropometry

The coefficients of the statistical model for height and BMI were around 1.1, which meant that the size of the error tended to increase with the size of the person, such that for an increment of one standard deviation of those variables, the error typically increased 10%. The coefficients for sex were usually smaller than 1, with mean value around 0.89; therefore, the error for male subjects was typically 11% smaller than for female of the same size. The study [19] also found differences in subjects with different BMIs, although only the error in ASIS was significant.

5. Conclusion

We have developed an automatic markerless procedure to identify the studied ALs from a homologous mesh. For the majority of AL, the SNV was typically 2 or 3 vertices away from the best possible representation of the landmark in the mesh. Published data about reliability of AL positioning by manual palpation was very variable, so depending on the source, the errors that we obtained were smaller than inter-examiner errors for most landmarks, or up to 2 or 3 times greater. We have also modelled the variation of those errors with sex, height and BMI. We found that the error increased 5% and 10% with the increment of one standard deviation of height and BMI respectively, and that the error for male subjects was 11% smaller in ML axis and 4% smaller in V and AP axes than for female subjects of the same size.

It is important to highlight that this is a starting point in the development of a markerless system using the homologous mesh properties.

Future work will be focused on analysing if this procedure to determine the AL could be used for motion analysis, without significantly increasing the errors.

Declaration of interest

None.

References

[1] U. Della Croce, A. Leardini, L. Chiari, A. Cappozzo, Human movement analysis using stereophotogrammetry: Part 4: assessment of anatomical landmark misplacement and its effects on joint kinematics, Gait & Posture. 21 (2005) 226–237. https://doi.org/10.1016/j.gaitpost.2004.05.003.

[2] R.S. Razavian, S. Greenberg, J. McPhee, Biomechanics Imaging and Analysis, in: R. Narayan (Ed.), Encyclopedia of Biomedical Engineering, Elsevier, Oxford, 2019: pp. 488–500. https://doi.org/10.1016/B978-0-12-801238-3.99961-6.

[3] R.M. Kanko, E.K. Laende, E.M. Davis, W.S. Selbie, K.J. Deluzio, Concurrent assessment of gait kinematics using marker-based and markerless motion capture, Journal of Biomechanics. 127 (2021) 110665. https://doi.org/10.1016/j.jbiomech.2021.110665.

[4] N. Nakano, T. Sakura, K. Ueda, L. Omura, K. Arata, Y. Iino, S. Fukashiro, S. Yoshioka, Evaluation of 3D Markerless Motion Capture Accuracy Using OpenPose With Multiple Video Cameras, Frontiers in Sports and Active Living. 2:50 (2020). https://doi.org/10.3389/fspor.2020.00050.

[5] E. Ceseracciu, Z. Sawacha, C. Cobelli, Comparison of Markerless and Marker-Based Motion Capture Technologies through Simultaneous Data Collection during Gait: Proof of Concept, PLOS ONE. 9 (2014) e87640. https://doi.org/10.1371/journal.pone.0087640.

[6] M.A. Perrott, T. Pizzari, J. Cook, J.A. McClelland, Comparison of lower limb and trunk kinematics between markerless and marker-based motion capture systems, Gait & Posture. 52 (2017) 57–61. https://doi.org/10.1016/j.gaitpost.2016.10.020.

[7] M. Moro, G. Marchesi, F. Hesse, F. Odone, M. Casadio, Markerless vs. Marker-Based Gait Analysis: A Proof of Concept Study, Sensors (Basel). 22(5):2011 (2022). https://doi.org/10.3390/s22052011.

[8] E. Parrilla, A. Ballester, P. Parra, A. Ruescas, J. Uriel, D. Garrido, S. Alemany, MOVE 4D: Accurate High-Speed 3D Body Models in Motion, in: Proc. of 3DBODY.TECH 2019, Lugano, Switzerland, 2019: pp. 30–32. https://doi.org/doi:10.15221/19.030.

[9] A.V. Ruescas Nicolau, H. De Rosario, F.B. Della-Vedova, E.P. Bernabé, M.-C. Juan, J. López-Pascual, Accuracy of a 3D Temporal Scanning System for Gait Analysis: Comparative With a Marker-based Photogrammetry System, Gait & Posture. 97 (2022) 28–34. https://doi.org/10.1016/j.gaitpost.2022.07.001.

[10] K.M. Robinette, S. Blackwell, H. Daanen, M. Boehmer, S. Fleming, Civilian American and European Surface Anthropometry Resource (CAESAR), Final Report. Volume 1. Summary, SYTRONICS INC DAYTON OH, 2002. https://apps.dtic.mil/sti/citations/ADA406704 (accessed February 16, 2022).

[11] A. Ballester, A. Pierola, E. Parrilla, J. Uriel, A.V. Ruescas, C. Perez, J.V. Dura, S. Alemany, 3D Human Models from 1D, 2D and 3D Inputs: Reliability and Compatibility of Body Measurements, in: Proc. of 3DBODY.TECH 2018, Lugano, Switzerland, 2018: pp. 132–141. https://doi.org/10.15221/18.132.

[12] D. Anguelov, P. Srinivasan, D. Koller, S. Thrun, J. Rodgers, J. Davis, SCAPE: shape completion and animation of people, in: ACM Transactions on Graphics (TOG), ACM, 2005: pp. 408–416.

[13] Anthropometric Relationships of Body and Body Segment Moments of Inertia, n.d. https://apps.dtic.mil/sti/citations/ADA097238 (accessed November 24, 2022).

[14] J. Fairbanks, M. Besançon, S. Simon, J. Hoffiman, N. Eubank, S. Karpinski, JuliaGraphs/Graphs.jl: an optimized graphs package for the Julia programming language, (2021). https://github.com/JuliaGraphs/Graphs.jl/.

[15] P.K. Dunn, G.K. Smyth, dglm: Double Generalized Linear Models, 2020. https://CRAN.R-project.org/package=dglm (accessed November 13, 2022).

[16] G.K. Smyth, Generalized Linear Models with Varying Dispersion, Journal of the Royal Statistical Society. Series B (Methodological). 51 (1989) 47–60.

[17] D. Burnsides, M. Boehmer, K. Robinette, 3-D landmark detection and identification in the CAESAR project, in: Proceedings Third International Conference on 3-D Digital Imaging and Modeling, 2001: pp. 393–398. https://doi.org/10.1109/IM.2001.924485.

[18] U. Della Croce, A. Cappozzo, D.C. Kerrigan, Pelvis and lower limb anatomical landmark calibration precision and its propagation to bone geometry and joint angles, Med. Biol. Eng. Comput. 37 (1999) 155–161. https://doi.org/10.1007/BF02513282.

[19] C.S. Moriguchi, L. Carnaz, L.C.C.B. Silva, L.E.B. Salasar, R.L. Carregaro, T. de O. Sato, H.J.C.G. Coury, Reliability of intra- and inter-rater palpation discrepancy and estimation of its effects on joint angle measurements, Manual Therapy. 14 (2009) 299–305. https://doi.org/10.1016/j.math.2008.04.002.

[20] P. Salvia, S.V.S. Jan, A. Crouan, L. Vanderkerken, F. Moiseev, V. Sholukha, C. Mahieu, O. Snoeck, M. Rooze, Precision of shoulder anatomical landmark calibration by two approaches: A CAST-like protocol and a new anatomical palpator method, Gait & Posture. 29 (2009) 587–591. https://doi.org/10.1016/j.gaitpost.2008.12.013.

[21] M. Kouchi, M. Mochimaru, Errors in landmarking and the evaluation of the accuracy of traditional and 3D anthropometry, Applied Ergonomics. 42 (2011) 518–527. https://doi.org/10.1016/j.apergo.2010.09.011.

[22] Z.B. Azouz, C. Shu, A. Mantel, Automatic Locating of Anthropometric Landmarks on 3D Human Models, in: Third International Symposium on 3D Data Processing, Visualization, and Transmission (3DPVT'06), 2006: pp. 750–757. https://doi.org/10.1109/3DPVT.2006.34.